Received: 30 May 2018 | Revised: 19 June 2018 | Accepted: 19 June 2018

DOI: 10.1002/poc.3888

RESEARCH ARTICLE

WILEY Journal of Physical Organic Chemistry

Stereoselectivity in a series of 7-alkylbicyclo[3.2.0]hept-2-enes: Experimental and computational perspectives

Phyllis Leber | Katherine Kidder | Don Viray | Eric Dietrich-Peterson | Yuan Fang | Alexander Davis

Department of Chemistry, Franklin & Marshall College, Lancaster, PA, USA

Correspondence
Phyllis Leber, Department of Chemistry, Franklin & Marshall College, Lancaster, PA 17604-3003, USA.
Email: pleber@fandm.edu

Funding information
Franklin & Marshall College Hackman Fund; American Chemical Society Petroleum Research Fund, Grant/Award Number: 55266-UR4

Abstract

Rate constants for overall decomposition (k_d) for a series of *exo*-7-alkylbicyclo[3.2.0]hept-2-enes are relatively invariant. For the alkyl substituents ethyl, propyl, butyl, isopropyl, and *t*-butyl, the ratio of the rate constant for [1,3] sigmatropic rearrangement to the rate constant for fragmentation, k_{13}/k_f, is significantly lower than $k_{13}/k_f = 150$ observed for *exo*-7-methylbicyclo[3.2.0]hept-2-ene. Regardless of the size and mass of the alkyl group, the stereoselectivity of the [1,3] carbon migration appears to be quite stable at 80% to 89% suprafacial inversion (*si*), an observation consistent with conservation of angular momentum but not conservation of orbital symmetry. This global result comports with the phenomenon of "dynamic matching" espoused by Carpenter and collaborators for [1,3] sigmatropic rearrangements in general.

KEYWORDS

[1,3] carbon migration, [1,3] sigmatropic rearrangement, bicyclo[3.2.0]hept-2-enes, computational analysis, first-order kinetics, vinylcyclobutane thermal chemistry

1 | INTRODUCTION

Bicyclo[3.2.0]hept-2-ene (**1**) undergoes thermal isomerization to norbornene (**2**) in the gas phase. This rearrangement has served as a historical exemplar of a [1,3] sigmatropic carbon migration. Competitive isomerization and fragmentation processes at temperatures in excess of 300°C convert **1** to its isomer **2** or directly to fragments cyclopentadiene and ethylene (Scheme 1).[1,2] Determination of an accurate rate constant k_{13} for the [1,3] rearrangement **1**-to-**2** and the associated Arrhenius parameters is complicated by the observation that **2** experiences facile Diels-Alder cycloreversion (retro Diels-Alder reaction) to cyclopentadiene and ethylene. Despite the large experimental error in activation energy for the [1,3] process, Cock and Frey conclude that the activation parameters for the sum ($k_{13} + k_f$) are close to the expected values "if both processes have a biradical mechanism" and therefore that "a two-step pathway is competitive."[1]

1.1 | Criteria of concert: energetics and stereoselectivity

Given the dramatic impact surrounding the publication of *The Conservation of Orbital Symmetry* the previous year, the tone of the Cocks and Frey paper is all the more remarkable. Woodward and Hoffmann recognized that a "two step, non-concerted path"[3] for the [1,3] sigmatropic rearrangement of vinylcyclopropane to cyclopentene was thermodynamically consistent with an activation energy ca. 50 kcal/mol, a value virtually identically to that reported by Cocks and Frey. Indeed, of the

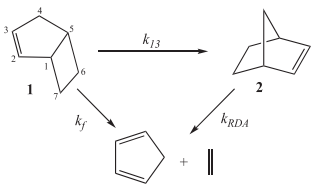

SCHEME 1 Thermal reactions of bicyclo[3.2.0]hept-2-ene (**1**)

two criteria for concert—energetics and stereoselectivity—explicated by Gajewski, [1,3] sigmatropic rearrangements have never satisfied the energetic criterion due to their high activation energies.[4]

However, Woodward and Hoffmann declared emphatically that Berson and Nelson,[5] in their study of *exo*-7-d-*endo*-6-acetoxybicyclo[3.2.0]hept-2-ene (Equation 1), made a "dramatic observation that [it] undergoes a concerted symmetry-allowed suprafacial [1,3] shift, *with inversion at the migrating center*, ... at 307°C."[3] Due to the steric inhibition of antarafacial migration in bicyclo[3.2.0]hept-2-enes, only suprafacial migration is geometrically feasible. According to the Woodward-Hoffmann rules, suprafacial migration with inversion of configuration (*si*) is privileged as orbital-symmetry allowed and suprafacial migration with retention of configuration (*sr*) is orbital-symmetry forbidden. The mechanistic debate about whether the [1,3] sigmatropic rearrangement is concerted or stepwise has therefore primarily focused on stereochemical outcomes in cases where the migrating center, C7 of bicyclo[3.2.0]hept-2-ene **1**, carries a substituent to enable differentiation between the *si* and *sr* products. Thus, *si/sr* ratios such as *si/sr* ≥ 19 as reported by Berson and Nelson have been cited as a measure of the degree of orbital symmetry control in [1,3] sigmatropic rearrangements.

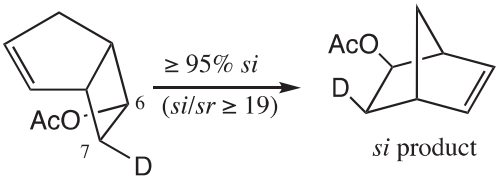

(eqn 1)

As more experimental evidence has been compiled for negligible stereoselectivity, by examining the more conformationally flexible bicyclo[4.2.0]oct-2-enes, the mechanistic viewpoint has gained prominence that [1,3] sigmatropic rearrangements traverse short-lived diradical transition structures residing on a shallow energy surface.[6] The mixed stereochemical results that have often converged toward a value of unity have effectively subverted alternative mechanistic interpretations such as competing orbital symmetry-allowed (*si*) and orbital symmetry-forbidden (sr) pathways [7] or competing concerted (*si*) and diradical (*si*/*sr*) mechanisms.[8] The potential, however, for a short-lived nonequilibrated diradical intermediate to partition between inversion and retention modes[9] deserves more critical examination.

1.2 | Computational studies

Based on extensive direct dynamics calculations of bicyclo[3.2.0]hept-2-ene (**1**) as well as its *exo*-7-methyl and *endo*-7-methyl analogs, Carpenter has predicted that the *exo*-7-methyl analog will bifurcate between inversion and retention products.[10] These mixed stereochemical results, however, are dynamic in origin and independent of orbital symmetry control. The dynamic model produces a local energy minimum corresponding to a transient diradical intermediate for the **1**-to-**2** interconversion. Carpenter has attributed the dominance of the *si* product to the contribution of C6-C7 bond rotation with a directional bias during the C1-C7 bond-breaking process. Transient bonding interaction between the orbital on the migrating carbon C7 and the orbital on C1 governs this C6-C7 rotational bias. Carpenter further postulated that conservation of angular momentum propels the migrating carbon C7 toward the migration terminus C3 with a strong preference for inversion of configuration.

Theoretical treatments of bicyclo[3.2.0]hept-2-enes have elucidated other mechanistic variables that impact [1,3] carbon migrations. Using CASSCF computational methods with a 6-31G* basis set, Houk's model of the **1**-to-**2** transformation implicated diradical transition structures on a broad shallow potential energy surface.[11] The preferred *si* pathway has been computed to be ca. 1 kcal/mol lower in energy than the *sr* pathway. Houk therefore proposed that the inherent shape of the potential energy surface as dictated by optimized geometries for stationary points is sufficient to account for the dominance of the *si* product. Houk has further suggested that repulsive interactions between the p orbital on C7, the migrating center, and the C2-C3 π bond cause rotational barriers that favor motion resulting in inversion.[12]

A more recent reappraisal of the intrinsic reaction coordinate for the **1**-to-**2** conversion using the B3LYP DFT method and a 6-31G* basis set confirms the dominance of singlet diradical structures on the plateau of the potential energy profile. Monitoring changes in the spin-coupled wave functions for the *si* pathway as the reacting orbitals evolved over time, Karadakov and Cooper observed "the dominance of singlet diradical character over an extended range of geometries."[13]

Carpenter[14] recently examined singlet diradicals that reside on a caldera, a broad shallow energy plateau.

Although Carpenter proposes that these diradical species possess small amounts of excess energy, the "exact distribution" of this energy is highly influential on the product distributions. Carpenter and collaborators[15] have also correlated this "dynamic matching" phenomenon of a preferred exit channel related to the initial trajectory of the bond cleavage with a quantum mechanical analog, whereby the momentum of the probability electron density dictates the product outcome. This analysis is consistent with Carpenter's earlier assessment that the *si* product would form preferentially to the *sr* product in the [1,3] sigmatropic rearrangement of *exo*-7-methylbicyclo[3.2.0]hept-2-ene.

1.3 | Experimental study of *exo*-7-methylbicyclo[3.2.0]hept-2-ene

It has been 15 years since our report on the thermal rearrangement of *exo*-7-methylbicyclo[3.2.0]hept-2-ene (**3**) in the gas phase at 275°C (Scheme 2).[2] The dominant exit channel is [1,3] sigmatropic rearrangement to the methylnorbornenes with an *si/sr* ratio of 7. These results are consistent with one of the following mechanisms: (1) the intermediacy of a nonequilibrated singlet diradical, (2) competition between a concerted *si* and an equilibrated diradical, or (3) competition between concerted inversion and retention pathways. Carpenter suspected that there would be a temperature effect if an equilibrated diradical were competing with a concerted *si* mechanism; that is, more of the diradical would fragment to cyclopentadiene and propene, which for entropic reasons would become more favorable at higher temperatures.[10] Instead, we observed that the *si/sr* ratio is invariant over the temperature range 250°C to 300°C, thus negating mechanistic interpretation (2). If competing concerted processes were occurring, then the *si/sr* ratio for the methyl analog would be less than that of the parent **1** because Carpenter has predicted that **3** unlike **1** would experience such competing processes. Any contribution from the *sr* pathway would reduce the *si/sr* ratio for the *exo*-7-methyl analog **3** compared with the parent **1** with a suitably positioned deuterium label. Baldwin, however, reported an *si/sr* ratio of 3 for compound **1** with a deuterium label at C7. This observation effectively precludes mechanistic interpretation (3), so that the only plausible mechanistic rationale that remains from the results of this study is the intermediacy of a short-lived singlet diradical.

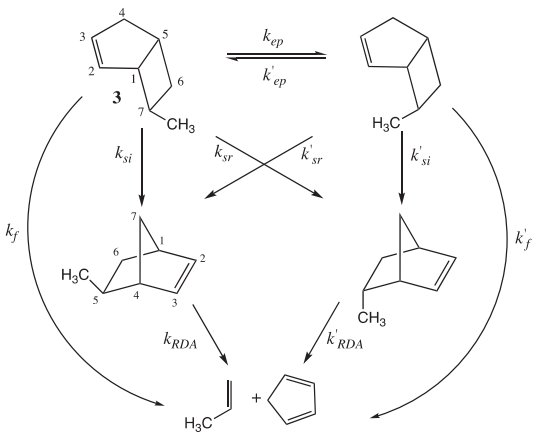

SCHEME 2 Thermal reactions of *exo*-7-methylbicyclo[3.2.0]hept-2-ene (**3**)

In comparing the *si/sr* ratios for the bicyclo[3.2.0]hept-2-enes and bicyclo[4.2.0]oct-2-enes,[16] in each case the *si/sr* ratio is higher when there is a methyl substituent versus a deuterium on the migrating center. The higher stereoselectivity observed for **3** versus that of deuterium-labeled **1** suggests that either steric factors or the moment of inertia about the C6-C7 bond might well influence the stereoselectivity of the [1,3] migration. It is this proposition that allowed us to reconsider our earlier assumption that all *exo*-7-alkylbicyclo[3.2.0]hept-2-enes would yield comparable results both kinetically and stereochemically.

1.4 | Computational study of *exo*-7-methylbicyclo[3.2.0]hept-2-ene

The [1,3] carbon migration of *exo*-7-methylbicyclo[3.2.0]hept-2-ene was examined using CASSCR, CASPT2, and CAS + 1 + 2 methods.[17] Based on these three methods, the transition states and diradical intermediate were determined to be within ca. 1 kJ/mol energetically, from which a caldera or shallow energy well on the potential energy surface can be inferred. Computed energy barriers are on the order of 188 to 196 kJ/mol. Tao and Fang also reported G2 values for their reactants and products, but not intermediates and transition states. This is likely due to a similar difficulty of the composite methods used in this study of converging to an optimized structure for the intermediates and transition state structures.

2 | EXPERIMENTAL

2.1 | Materials

All reagents and solvents were purchased from either Sigma-Aldrich or Fisher Scientific and were used without further purification except that, just prior to use, dicyclopentadiene was cracked to yield 1,3-cyclopentadiene and potassium *t*-butoxide was sublimed. Flash column chromatography was performed using silica gel (Sigma-Aldrich 100-200 mesh). Mass spectra to confirm molecular formulas and to record fragment ions

were determined using an Agilent Technologies 5973 mass selective detector and a 6890N Network GC System. NMR spectra were acquired on a Varian INOVA 500-MHz instrument. ^{13}C NMR hydrogen multiplicities for all compounds were obtained by DEPT pulse sequences. All GC analyses were acquired on an HP cross-linked methyl silicone column (50 m × 0.2 mm i.d. × 0.10 μm film thickness). Purification of samples for spectral characterization and for thermal reactions was accomplished by preparative GC on a 1/4 in × 12 ft DC-710 column.

2.2 | Syntheses

All of the *endo*-7-alkylbicyclo[3.2.0]hept-2-en-6-ones were prepared by ketene cycloaddition of 1,3-cyclopentadiene and the corresponding alkylketene, which was generated in situ by treatment of the corresponding acid chloride with triethylamine.[18] For all of the *endo*-7-alkylbicyclo[3.2.0]hept-2-en-6-ones **4**, the ^{13}C NMR chemical shift differential between the two sp^2-hybridized carbons is ca. 5.0 ppm except for the 2.4 ppm differential in *endo*-7-*t*-butylbicyclo[3.2.0]hept-2-en-6-one. Ketones **4** were purified via column chromatography using 9:1 pentane:ether as the eluting solvent. A low-temperature Wolff-Kishner protocol[19] involving initial conversion of each ketone to its hydrazone derivative followed by subsequent treatment with potassium *t*-butoxide yielded the corresponding *exo*-7-alkylbicyclo[3.2.0]hept-2-enes **5** (Scheme 3).[2] It should be noted that the basic conditions of this latter sequence resulted in epimerization at C7, the α-carbon.

Ethylnorbornene was obtained by subjecting acetylnorbornene, the Diels-Alder cycloadduct of cyclopentadiene and methyl vinyl ketone,[20] to a low-temperature Wolff-Kishner reduction (Scheme 4). As was observed with the 7-alkylbicyclo[3.2.0]hept-2-enes, epimerization occurred at the α-carbon to afford *exo*-5-ethylnorbornene as the dominant stereoisomer with an *exo*: *endo* ratio of 3:1.

Most of the 5-alkylnorbornenes, however, were obtained via Diels-Alder cycloaddition of cyclopentadiene and the appropriate alkene in a sealed tube[21] at temperatures in the range of 170°C to 190°C to give the *endo*-5-alkylnorbornene as the major product (Scheme 5) in an *exo*:*endo* ratio of ca. 1:4. ^{13}C NMR spectral data provided strong empirical evidence to differentiate the *endo*- and *exo*-5-alkylnorbornenes: a ca. 4 to 5 ppm shielding of the bridging methylene in the *exo*-5-alkylnorbornenes by

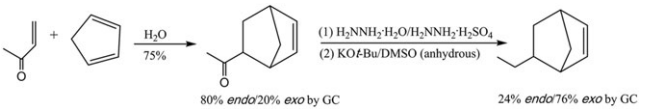

SCHEME 4 Synthetic scheme for 5-ethylnorbornenes

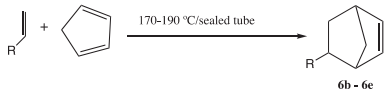

SCHEME 5 Synthetic scheme for *endo*-5-alkylnorbornenes

the alkyl group and a 4 to 5 ppm differential between the chemical shifts of the two sp^2-hybridized carbons in the *endo* epimer compared with a < 1 ppm differential in the *exo* epimer. For example, the bridging methylene in *exo*-5-ethylnorbornene resonates at 45.2 ppm; in *endo*-5-ethylnorbornene, at 49.6 ppm. The chemical shift differential between the two sp^2-hybridized carbons in *exo*-5-ethylnorbornene is 0.7 ppm; in *endo*-5-ethylnorbornene, 4.5 ppm. The exception to this pattern occurred for *endo*-5-*t*-butylnorbornene with an sp^2-hybridized carbon chemical shift differential of only 2.1 ppm, just as an sp^2-hybridized carbon chemical shift 2.4 ppm differential was observed for *endo*-7-*t*-butylbicyclo[3.2.0]hept-2-en-6-one.

endo-7-ethylbicyclo[3.2.0]hept-2-en-6-one (**4a**). **IR** (cm^{-1}) 3050, 2965, 1767, 700. **MS** (EI) *m/z* 136 (M, 1), 121 (1), 108 (20), 107 (4), 93 (7), 91 (13), 79 (42), 77 (28), 66 (100). **^{1}H NMR** (500 MHz, $CDCl_3$) ∂ 5.79 (d, 1 H), 5.69 (m, 1 H), 3.68 (m, 1 H), 3.52 (m, 1 H), 3.31 (m, 1 H), 2.55 (d, 1H), 2.30 (m, 1H), 1.51 (m, 1H), 1.30 (m, 1H), 0.87 (t, 3H). **^{13}C NMR** (125 MHz, $CDCl_3$, DEPT) ∂ 215.6 (C═O), 134.6 (═CH), 129.4 (═CH), 66.6 (CH), 58.9 (CH), 41.8 (CH), 33.8 (CH_2), 18.1 (CH_2), 11.9 (CH_3).

endo-7-propylbicyclo[3.2.0]hept-2-en-6-one (**4b**). **IR** (cm^{-1}) 3055, 2957, 1771, 701. **MS** (EI) *m/z* 150 (M, $C_{10}H_{14}O$, 1), 122 (15), 91 (9), 79 (25), 77 (16), 66 (100). **^{1}H NMR** (500 MHz, $CDCl_3$) ∂ 5.84 (m, 1H), 5.72 (m 1H), 3.75 (m, 1H), 3.56 (m, 1H), 3.42 (m, 1H), 2.60 (m, 1H), 2.35 (qq, 1H), 1.49 (m, 1H), 1.34 (m, 3H), 0.87 (t, 3H). **^{13}C NMR** (125 MHz, $CDCl_3$, DEPT) ∂ 216.0 (C═O), 134.7 (═CH), 129.8 (═CH), 64.9 (CH), 59.3 (CH), 42.2 (CH), 34.0 (CH_2), 27.0 (CH_2), 20.8 (CH_2), 14.0 (CH_3).

endo-7-butylbicyclo[3.2.0]hept-2-en-6-one (**4c**). **IR** (cm^{-1}) 3054, 2957, 1773, 701. **MS** (EI) *m/z* 164 (M,

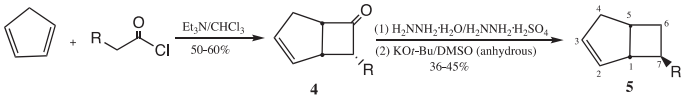

SCHEME 3 Synthetic scheme for *exo*-7-alkylbicyclo[3.2.0]hept-2-enes

$C_{11}H_{16}O$, 2), 136 (13), 91 (24), 79 (40), 77 (45), 66 (100). **^{1}H NMR** (500 MHz, $CDCl_3$) ∂ 5.82 (m, 1H), 5.70 (m 1H), 3.72 (m, 1H), 3.53 (m, 1H), 3.39 (m, 1H), 2.58 (m, 1H), 2.34 (m, 1H), 1.50 (m, 1H), 1.27 (m, 5H), 0.84 (t, 3H). **^{13}C NMR** (125 MHz, $CDCl_3$, DEPT) ∂ 215.7 (C═O), 134.7 (═CH), 129.7 (═CH), 65.2 (CH), 59.3 (CH), 42.3 (CH), 34.0 (CH_2), 29.8 (CH_2), 24.6 (CH_2), 22.6 (CH_2), 13.9 (CH_3).

endo-7-isopropylbicyclo[3.2.0]hept-2-en-6-one (**4d**). **IR** (cm^{-1}) 3054, 2954, 1766, 776, 704. **MS** (EI) *m/z* 150 (M, $C_{10}H_{14}O$, 1), 122 (14), 107 (6), 91 (8), 79 (22), 69 (34), 66 (100), 51 (4); **HRMS** (EI) calcd for $C_{10}H_{14}O$ (M 150.10447), found 150.10433. **^{1}H NMR** (500 MHz, $CDCl_3$) ∂ 5.85 (m, 1H), 5.81 (m, 1H), 3.71 (m, 1H), 3.57 (m, 1H), 3.10 (m, 1H), 2.63 (m, 1H), 2.38 (qq, 1H), 1.80 (m, 1H), 1.05 (d, 3H), 0.89 (d, 3H). **^{13}C NMR** (125 MHz, $CDCl_3$, DEPT) ∂ 214.7 (C═O), 134.7 (═CH), 129.9(═CH), 72.4 (CH), 58.6 (CH), 42.0 (CH), 33.8 (CH_2), 26.0 (CH), 21.13 (CH_3), 21.05 (CH_3).

endo-7-*t*-butylbicyclo[3.2.0]hept-2-en-6-one (**4e**). **IR** (cm^{-1}) 3040, 2951, 1764, 1461, 740. **MS** (EI) *m/z* 164 (M, 1), 136 (15), 122 (5), 108 (22), 91 (18), 83 (99), 77 (32), 66 (100). **^{1}H NMR** (500 MHz, $CDCl_3$) ∂ 5.90 (m, 1H), 5.78 (m, 1H), 3.65 (m, 1H), 3.60 (m, 1H), 3.36 (dd, 1H), 2.64 (br d, 1H), 2.36 (qq, 1H), 0.98 (s, 9H). **^{13}C NMR** (125 MHz, $CDCl_3$, DEPT) ∂ 213.2 (C═O), 133.3 (═CH), 131.0 (═CH), 75.3 (CH), 58.2 (CH), 42.9 (CH), 33.1 (CH_2), 32.4 (C), 28.5 (CH_3).

exo-7-ethylbicyclo[3.2.0]hept-2-ene (**5a**). **IR** (cm^{-1}) 3047, 2958, 1689, 711. **MS** (EI) *m/z* 122 (M, C_9H_{14}, 1), 93 (5), 91 (14), 79 (20), 77 (18), 67 (10), 66 (100). **^{1}H NMR** (500 MHz, $CDCl_3$) *exo*-**5a**: ∂ 5.77 (m, 1H), 5.73 (m, 1H), 2.84 (m, 1H), 2.55 (qq, 1H), 2.15 (m, 1H), 1.81 (m, 1H), 1.76 (m, 2H), 1.54 (m, 3H), 0.86 (t, 3H); *endo*-**5a**: ∂ 5.81 (m, 1H), 5.74 (m, 1H), 3.27 (br m, 2H), 2.68 (pent, 1H), 2.47 (m, 1H), 2.40 (p, 1H), 2.24 (dq, 1H), 2.06 (m, 1H), 1.30 (m, 1H), 1.22 (m, 1H), 0.76 (t, 3H). **^{13}C NMR** (125 MHz, $CDCl_3$, DEPT) *exo*-**5a**: ∂ 133.9 (═CH), 130.1 (═CH), 51.3 (CH), 43.4 (CH), 40.6 (CH_2), 32.8 (CH), 32.4 (CH_2), 29.4 (CH_2), 11.7 (CH_3); *endo*-**5a**: ∂ 132.1 (═CH), 131.0 (═CH), 49.5 (CH), 40.3 (CH), 40.2 (CH_2), 33.5 (CH_2), 32.2 (CH), 24.7 (CH_2), 11.7 (CH_3).

exo-7-propylbicyclo[3.2.0]hept-2-ene (**5b**). **IR** (cm^{-1}) 3049, 2955, 2924, 1664, 716. **MS** (EI) *m/z* 136 (M, $C_{10}H_{16}$, 2), 91 (7), 79 (13), 77 (8), 66 (100). **^{1}H NMR** (500 MHz, $CDCl_3$). ∂ 5.77 (m, 1H), 5.73 (m, 1H), 2.84 (br m, 2H), 2.55 (m, 1H), 2.15 (dt, 1H), 1.76 (q, 2H), 1.50 (m, 2H), 1.28 (m, 3H), 0.89 (t, 3H). **^{13}C NMR** (125 MHz, $CDCl_3$, DEPT) ∂ 133.9 (═CH), 130.1 (═CH), 51.5 (CH), 41.3 (CH), 40.6 (CH_2), 38.9 (CH_2), 32.74 (CH), 32.66 (CH_2), 20.4 (CH_2), 14.2 (CH_3).

exo-7-butylbicyclo[3.2.0]hept-2-ene (**5c**). **IR** (cm^{-1}) 3047, 2922, 706. **MS** (EI) *m/z* 150 (M, $C_{11}H_{18}$, 1), 91 (5), 79 (10), 77 (5), 66 (100). **^{1}H NMR** (500 MHz, $CDCl_3$). ∂ 5.76 (m, 1H), 5.73 (m, 1H), 2.83 (br m, 2H), 2.55 (m, 1H), 2.15 (dp, 1H), 1.90 (m, 1H), 1.76 (m, 2H), 1.52 (m, 2H), 1.31 (p, 2H), 1.23 (m, 2H), 0.90 (t, 3H). **^{13}C NMR** (125 MHz, $CDCl_3$, DEPT) *exo*-**5c**: ∂ 133.9 (═CH), 130.1 (═CH), 51.6 (CH), 41.6 (CH), 40.6 (CH_2), 36.3 (CH_2), 32.73 (CH), 32.69 (CH_2), 29.6 (CH_2), 22.8 (CH_2), 14.2 (CH_3); *endo*-**5c**: ∂ 132.0 (═CH), 131.2 (═CH), 49.7 (CH), 40.2 (CH_2), 38.5 (CH), 33.8 (CH_2), 32.5 (CH), 31.5 (CH_2), 29.7 (CH_2), 22.8 (CH_2), 14.2 (CH_3).

exo-7-isopropylbicyclo[3.2.0]hept-2-ene (**5d**). **IR** (cm^{-1}) 3048, 2952, 720. **HRMS** (EI) calcd for $C_{10}H_{16}$ (M 136.1252), found 136.1258. **^{1}H NMR** (500 MHz, $CDCl_3$) *exo*-**5d**: ∂ 5.73 (m, 2H), 2.93 (br s, 1H), 2.70 (m, 1H), 2.54 (dd, 1H), 2.14 (d, 1H), 1.65 (m, 2H), 1.45 (m, 2H), 0.86 (d, 3H), 0.80 (d, 3H); *endo*-**5d**: ∂ 0.78 (d, 3H), 0.66 (d, 3H). **^{13}C NMR** (125 MHz, $CDCl_3$, DEPT) *exo*-**5d**: ∂ 134.2 (═CH), 130.0 (═CH), 49.8 (CH), 49.7 (CH), 40.7 (CH_2), 32.9 (CH), 32.1 (CH), 30.9 (CH_2), 19.8 (CH_3), 19.5 (CH_3); *endo*-**5d**: ∂ 131.9 (═CH), 131.1 (═CH), 49.1 (CH), 46.5 (CH), 40.1 (CH_2), 32.6 (CH_2), 31.3 (CH), 30.0 (CH), 20.4 (CH_3), 19.2 (CH_3).

exo-7-*t*-butylbicyclo[3.2.0]hept-2-ene (**5e**). **IR** (cm^{-1}) 3056, 2930, 727. **MS** (EI) *m/z* 150 (M, $C_{11}H_{18}$, 6), 109 (8), 91 (18), 79 (31), 77 (18), 66 (100). **^{1}H NMR** (500 MHz, $CDCl_3$) *exo*-**5e**: ∂ 5.73 (m, 2H), 2.98 (br s, 1H), 2.60 (p, 1H), 2.55 (m, 1H), 2.17 (m, 1H), 1.98 (m, 1H), 1.77 (m, 1H), 1.60 (m, 1H), 0.87 (s, 9H); *endo*-**5e**: ∂ 0.81 (s, 9H). **^{13}C NMR** (125 MHz, $CDCl_3$, DEPT) ∂ 134.6 (═CH), 129.9 (═CH), 53.2 (CH), 47.4 (CH), 40.7 (CH_2), 32.5 (CH), 31.8 (C), 28.3 (CH_2), 26.2 (CH_3).

exo-5-ethylbicyclo[2.2.1]hept-2-ene (**6a**). **IR** (cm^{-1}) 3061, 2921, 703. **MS** (EI) *m/z* 122 (M, C_9H_{14}, 12), 91 (22), 77 (31), 66 (100). **^{1}H NMR** (500 MHz, $CDCl_3$) *exo*-**6a**: ∂ 6.06 (m, 1H), 6.00 (m, 1H), 2.76 (br s, 1H), 2.51 (br s, 1H), 1.38 (m, 2H), 1.28 (m, 2H), 1.23 (m, 2H), 1.05 (m, 1H), 0.91 (t, 3H); *endo*-**6a**: ∂ 0.85 (t, 3H). **^{13}C NMR** (125 MHz, $CDCl_3$, DEPT) *exo*-**6a**: ∂ 136.94 (═CH), 136.2 (═CH), 46.0 (CH), 45.2 (CH_2), 41.8 (CH), 40.9 (CH), 32.9 (CH_2), 29.3 (CH_2), 13.3 (CH_3). *endo*-**6a**: ∂ 136.87 (═CH), 132.4 (═CH), 49.6 (CH_2), 45.1 (CH), 42.5 (CH), 40.8 (CH), 32.2 (CH_2), 27.6 (CH_2), 13.0 (CH_3).

endo-5-propylbicyclo[2.2.1]hept-2-ene (**6b**). **IR** (cm^{-1}) 3046, 2931, 708. **MS** (EI) *m/z* 136 (M, $C_{10}H_{16}$, 6), 91 (5), 79 (6), 77 (5), 67 (5), 66 (100). **^{1}H NMR** (500 MHz, $CDCl_3$) *endo*-**6b**: ∂ 6.07 (dd, 1H), 5.89 (dd, 1H), 2.73 (br m, 2H), 1.95 (m, 1H), 1.81 (ddd, 1H), 1.30 (m, 3H), 1.24 (d, 1H), 1.05 (m, 2H), 0.85 (t, 3H), 0.46 (m, 1H); *exo*-**6b**: ∂ 0.88 (t, 3H). **^{13}C NMR** (125 MHz, $CDCl_3$, DEPT) *endo*-**6b**: ∂ 136.8 (═CH), 132.5 (═CH), 49.6 (CH_2), 45.4 (CH), 42.5 (CH), 38.5 (CH), 37.1 (CH_2), 32.4 (CH_2), 21.7

(CH_2), 14.4 (CH_3); *exo*-**6b**: ∂ 136.9 (=CH), 136.1 (=CH), 46.3 (CH), 45.2 (CH_2), 41.9 (CH), 38.9 (CH_2), 38.47 (CH), 33.0 (CH_2), 21.9 (CH_2), 14.4 (CH_3).

endo-5-butylbicyclo[2.2.1]hept-2-ene (**6c**). **IR** (cm^{-1}) 3056, 2930, 715. **MS** (EI) *m/z* 150 (M, $C_{11}H_{18}$, 5), 91 (5), 79 (6), 77 (5), 67 (6), 66 (100). **^{1}H NMR** (500 MHz, $CDCl_3$) ∂ 6.09 (dd, 1H), 5.91 (dd, 1H), 2.75 (br s, 1H), 2.73 (br s, 1H), 1.96 (m, 1H), 1.83 (ddd, 1H), 1.37 (m, 1H), 1.27 (m, 5H), 1.08 (m, 2H), 0.87 (t, 3H), 0.48 (m, 1H). **^{13}C NMR** (125 MHz, $CDCl_3$, DEPT) *endo*-**6c**: ∂ 136.8 (=CH), 132.5 (=CH), 49.6 (CH_2), 45.4 (CH), 42.5 (CH), 38.7 (CH), 34.5 (CH_2), 32.5 (CH_2), 30.9 (CH_2), 23.0 (CH_2), 14.2 (CH_3); *exo*-**6c**: ∂ 137.0 (=CH), 136.2 (=CH), 46.4 (CH), 45.2 (CH_2), 41.9 (CH), 41.5 (CH), 36.3 (CH_2), 33.1 (CH_2), 31.1 (CH_2), 23.0 (CH_2),14.2 (CH_3).

endo-5-isopropylbicyclo[2.2.1]hept-2-ene (**6d**). **IR** (cm^{-1}) 3048, 2927, 713. **MS** (EI) *m/z* 136 (M, $C_{10}H_{16}$, 5), 91 (5), 80 (6), 79 (6), 77 (5), 69 (1), 67 (10), 66 (100). **^{1}H NMR** (500 MHz, $CDCl_3$) ∂ 6.08 (m, 1H), 5.90 (m, 1H), 2.82 (br s, 1H), 2.72 (br s, 1H), 1.78 (m, 1H), 1.56 (m, 1H), 1.34 (m, 1H), 1.17 (d, 1H), 0.95 (d, 1H), 0.88 (d, 3H), 0.80 (d, 3H), 0.58 (m, 1H). **^{13}C NMR** (125 MHz, $CDCl_3$, DEPT) ∂ 137.1 (=CH), 132.1 (=CH), 49.4 (CH_2), 47.6 (CH), 44.6 (CH), 42.5 (CH), 32.8 (CH), 31.6 (CH_2), 22.0 (CH_3), 21.7 (CH_3).

endo-5-t-butylbicyclo[2.2.1]hept-2-ene (**6e**). **IR** (cm^{-1}) 3045, 2931, 702. **MS** (EI) *m/z* 150 (M, $C_{11}H_{18}$, 3), 109 (2), 91 (4), 80 (5), 79 (6), 77 (4), 66 (100). **^{1}H NMR** (500 MHz, $CDCl_3$) ∂ 5.99 (m, 1H), 5.90 (m, 1H), 2.82 (br s, 1H), 2.71 (br s, 1H), 1.90 (m, 1H), 1.70 (m, 1H), 1.29 (m, 3H), 0.76 (s, 9H). **^{13}C NMR** (125 MHz, $CDCl_3$, DEPT) ∂ 135.2 (=CH), 133.1 (=CH), 51.5 (CH_2), 50.7 (CH), 44.8 (CH), 42.4 (CH), 32.5 (C), 29.3 (CH_3), 27.6 (CH_2).

2.3 | Thermal reactions

All kinetic analyses were performed on samples that had been purified by preparative GC to ≥99% purity. The thermal reactions of *exo*-7-alkylbicyclo[3.2.0]hept-2-enes and mixtures of *endo*- and *exo*-5-alkylnorbornenes were followed at 275°C in sealed base-treated capillary tubes that had been subjected to three freeze-pump-thaw cycles prior to closure. Capillary GC analysis provided relative concentration versus reaction time data for the reactants and for all isomeric products. All components were well-resolved and eluted in the following order: *endo*-5-alkylnorbornenes < *exo*-5-alkylnorbornenes < *exo*-7-alkylbicyclo[3.2.0] hept-2-enes < *endo*-7-alkylbicyclo[3.2.0]hept-2-enes < internal standard (ISTD). The value of the rate constant for overall decomposition (k_d) of each *exo*-7-alkylbicyclo[3.2.0]hept-2-ene was obtained using the Solver function in Microsoft Excel to fit experimental concentrations to the first-order exponential rate expression based on the kinetic profile shown in Scheme 6 for *exo*-7-isopropylbicyclo[3.2.0]hept-2-ene.

The values of k_{si} and k_{sr} were also derived from a Solver curve fit of experimental and calculated concentrations of the transient 5-alkylnorbornenes. The rate constants for Diels-Alder cycloreversions were obtained experimentally by following the rate of disappearance of each 5-alkylnorbornene stereoisomer in a mixture of *endo*- and *exo*-5-alkylnorbornenes.

2.4 | Gaussian calculations

All geometry optimizations and frequency calculations were performed using the Gaussian09 suite of programs.[22] Conformational analysis was performed by optimizing all possible geometry conformers using the B3LYP/6-31 + G (d,p) method.[23,24] All conformers within 2.5 kJ/mol of the lowest energy conformer were then refined using the B3LYP/6-311++G(3df,3pd) method. The resulting lowest energy conformer was then used for all subsequent calculations. The energies were further refined using the CBS-QB3, G3, and G4 composite methods.[25–27] Enthalpy of formation values were determined by averaging six values, from two sets of isodesmic reactions (Table S1) for each of the three composite methods. Somers and Simmie have shown that this type of treatment leads to 95% confidence intervals of approximately 4 kJ/mol for the average of the composite methods selected here.[28] Transition states were confirmed by the presence of a single negative frequency that corresponded to the reaction path of interest. Rate constants (Table S2) were fit to a three-parameter Arrhenius expression over the temperature range of 400 to 600 K using the ChemRate software.[29] Hindered rotors were incorporated using a 1D Pitzer and Gwinn treatment, via rotational scans in 10° increments using the B3LYP/6-31 + G (d,p) method.[30] Due to difficulty in obtaining an optimized structure for the intermediates and transition states for the epimerization and inversion reactions, the computational values reported here will be limited

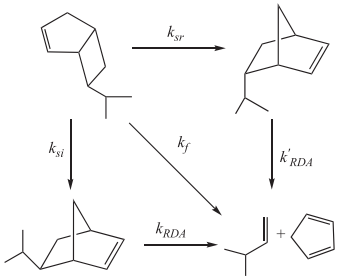

SCHEME 6 Thermal reactions of *exo*-7-isopropylbicyclo[3.2.0] hept-2-ene

to the *exo*- and *endo*-7-alkylbicyclo[3.2.0]hept-2-enes, the *exo*- and *endo*-5-alkylnorbornenes, and the products and transition states of the retro Diels-Alder reaction.

3 | RESULTS AND DISCUSSION

Representative rate constants for *exo*-7-isopropylbicyclo[3.2.0]hept-2-ene and the 7-isopropylnorbornenes, based on the thermal profile shown in Scheme 6, are as follows: $k_d = 1.1 \times 10^{-5}$ s^{-1}, $k_{si} = 6.5 \times 10^{-6}$ s^{-1}, $k_{sr} = 8.1 \times 10^{-7}$ s^{-1}, $k_{RDA} = 1.7 \times 10^{-4}$ s^{-1}, and $k'_{RDA} = 4.6 \times 10^{-4}$ s^{-1}. The *si*/*sr* value derived from k_{si} and k_{sr} is 8, and $k_{13} = k_{si} + k_{sr} = 7.3 \times 10^{-6}$ s^{-1}. The difference $k_d - k_{13}$ approximated k_f as 3.7×10^{-6} s^{-1}. The relative order of importance of kinetic processes is $k_{13} > k_f$ (Table 1).

The rates of retro Diels-Alder reactions for all *exo*-5-alkylnorbornenes were comparable as were those for the *endo*-5-alkylnorbornenes. In all cases, the reactivity of the *endo*-5-alkylnorbornenes exceeded that of the corresponding *exo*-5-alkylnorbornenes by a factor greater than 2 (Table 2).

The rate constants for the overall rate of decomposition (k_d) for a series of *exo*-7-alkylbicyclo[3.2.0]hept-2-enes are listed in Table 1 from the most reactive *exo*-7-propylbicyclo[3.2.0]hept-2-ene to the least reactive *exo*-7-isopropylbicyclo[3.2.0]hept-2-ene. Given that all of the *exo*-7-alkylbicyclo[3.2.0]hept-2-enes afford a secondary alkyl-allyl diradical upon homolytic cleavage of the C1-C7 bond (Scheme 7), it is not surprising that the k_d values for the most reactive entry are less than a factor of two greater than the least reactive entry (Table 1).

The computational results for the retro Diels-Alder reaction (Table 3) yielded values that are in reasonable agreement with the experimental ones (Table 2) reported here. The computational rates are between a factor of 1.7 and 3.7 times higher than the corresponding experimental values. However, because they are consistently higher, the k'_{RDA}/k_{RDA} ratios remain virtually the same, with the exception of the ethyl and *t*-butyl groups, where the k'_{RDA}/k_{RDA} is roughly 1.5 to 1.7 times higher. This confirms the finding that the *endo*-5-alkylnorbornenes undergo a more facile retro Diels-Alder reaction compared with their *exo*-5-alkylnorbornene counterparts, with the

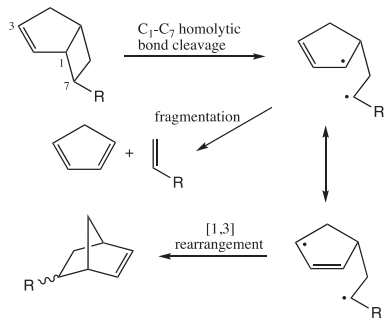

SCHEME 7 Bifurcation of 2° alkyl-allyl diradical between rearrangement and fragmentation

TABLE 1 Experimental rate constants and exit channels for *exo*-7-alkylbicyclo[3.2.0]hept-2-enes @ 275°C

R-	k_d @ 275°C	k_{rel}	k_{13}/k_f	% [1,3]	% epim	% frag
Pr-	2.0(±0.1) ×10^{-5} s^{-1}	1.8	3.2	76	0	24
Bu-	1.9(±0.1) ×10^{-5} s^{-1}	1.7	1.8	64	0	36
Et-	1.6(±0.1) ×10^{-5} s^{-1}	1.5	5.4	84	0	16
Me-	1.5(±0.2) ×10^{-5} s^{-1}	1.4	150	95	4	0.6
t-Bu-	1.4(±0.1) ×10^{-5} s^{-1}	1.3	2.9	74	0	26
i-Pr-	1.1(±0.1) ×10^{-5} s^{-1}	1.0	1.9	65	0	35

TABLE 2 Experimental rates of retro Diels-Alder reactions for *exo*- (k_{RDA}) and *endo*- (k'_{RDA})-5-alkylnorbornenes @ 275°C

R-	k_{RDA}	k'_{RDA}	k'_{RDA}/k_{RDA}
Et-	2.5(±0.1) ×10^{-4} s^{-1}	5.5(±0.3) ×10^{-4} s^{-1}	2.2
Me-	2.0(±0.1) ×10^{-4} s^{-1}	4.7(±0.2) ×10^{-4} s^{-1}	2.3
Pr-	2.5(±0.1) ×10^{-4} s^{-1}	6.0(±0.1) ×10^{-4} s^{-1}	2.4
i-Pr-	1.7(±0.1) ×10^{-4} s^{-1}	4.6(±0.1) ×10^{-4} s^{-1}	2.7
Bu-	1.8(±0.1) ×10^{-4} s^{-1}	5.0(±0.1) ×10^{-4} s^{-1}	2.8
t-Bu-	9.4(±0.8) ×10^{-5} s^{-1}	6.1(±0.2) ×10^{-4} s^{-1}	6.5

TABLE 3 Computational rates of retro Diels-Alder reactions for *exo*- (k_{RDA}) and *endo*- (k'_{RDA})-5-alkylnorbornenes

R-	k_{RDA}	k'_{RDA}	k'_{RDA}/k_{RDA}
Et-	4.4×10^{-4} s^{-1}	1.4×10^{-3} s^{-1}	3.1
Me-	6.5×10^{-4} s^{-1}	1.4×10^{-3} s^{-1}	2.2
Pr-	6.2×10^{-4} s^{-1}	1.5×10^{-3} s^{-1}	2.4
i-Pr-	3.1×10^{-4} s^{-1}	1.0×10^{-3} s^{-1}	3.3
Bu-	6.8×10^{-4} s^{-1}	1.8×10^{-3} s^{-1}	2.6
t-Bu-	1.9×10^{-4} s^{-1}	2.1×10^{-3} s^{-1}	11.

bulkier isopropyl and *t*-butyl substituents experiencing the greatest difference in susceptibility to cycloreversion.

One possible explanation for k'_{RDA} being greater than k_{RDA} is based on transition state comparisons (Figure 1). As the reaction proceeds, both C5 and C6 begin to assume more sp^2 character, which reduces the separation between these carbon atoms and the five-membered ring. For unbranched alkyl groups, the alkyl chain is pointed away from the transition state (Figure 1A,C), thereby minimizing steric interactions with the ring structure. The distances between the hydrogens on C5 and C7 and between those on C8 and C4 for the *endo* ethyl transition state are 2.481 and 2.856 Å, respectively (Figure 1A). For the *exo* ethyl epimer, the hydrogen distances of interest are between C8 and C7, and C8 and C4, which are 2.242 and 2.478 Å, respectively (Figure 1C). The closer distances on the *exo* epimer indicate stronger steric interactions, which help to explain why the rates for these reactions are lower for *exo*, even though the enthalpy of formation of the *exo* and *endo* epimers of 5-ethylnorbornene are very similar. In fact, the calculated enthalpy of formation for the retro Diels-Alder transition state of *exo*-5-ethylnorbornene is 5.23 kJ/mol higher than that of the *endo* epimer (Table 4).

For branched alkyl groups, the steric interactions are even more important. For the *endo*-5-isopropylnorbornene transition state, the distances between hydrogen atoms on C5 and C7, and C10 and C4 are 2.507 and 2.402 Å, respectively (Figure 1B). In the *exo* epimer, these same distances are 2.211 and 2.128 Å, respectively (Figure 1D). The further narrowing of these distances indicates a greater steric interaction that increases the energy of the transition state, thus affording differences in transition state enthalpy of formations of 10.4 and 11.0 kJ/mol for isopropyl and *t*-butyl,

TABLE 4 Difference in enthalpy of formation values between the *endo* and *exo* epimers of 7-methylbicyclo[3.2.0]hept-2-ene (**3**), of other 7-alkylbicyclo[3.2.0]hept-2-enes (**5**), of 5-alkylnorbornenes (**6**) and between the transition states for the retro Diels-Alder reaction of the 5-alkylnorbornenes (**6-RDA**). A negative value indicates that the *exo* epimer is more stable

	$\Delta\Delta H_f$, kJ/mol		$\Delta\Delta H_f^{\ddagger}$, kJ/mol
R-	3, 5	6	6-RDA
Me-	0.79	0.82	5.1
Et-	0.79	0.79	5.2
Pr-	0.95	1.67	5.2
Bu-	1.82	1.63	5.1
i-Pr-	3.68	4.15	10.4
t-Bu-	−5.72	−1.87	11.0

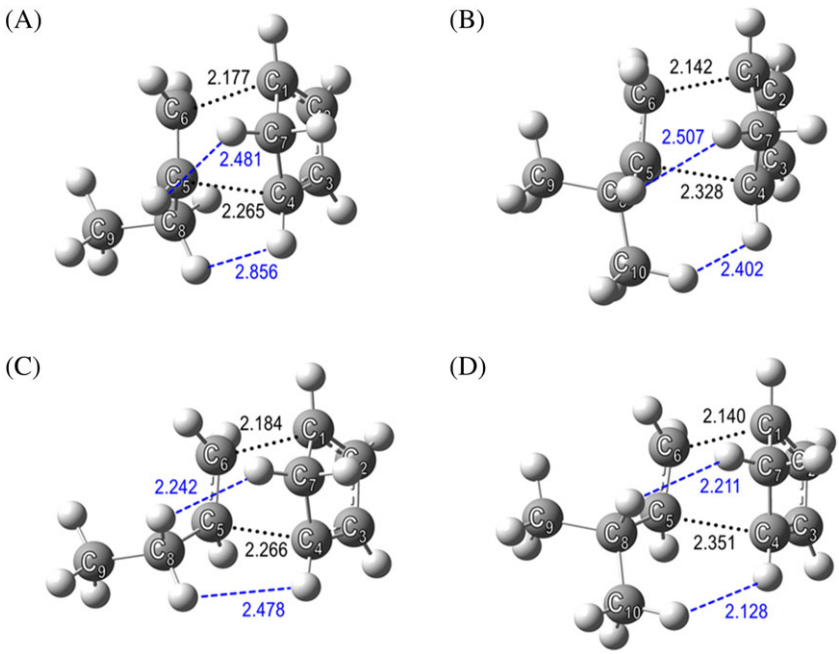

FIGURE 1 Molecular images with select geometric parameters for the retro Diels Alder transition state structures of (A) *endo*-5-ethylnorbornene, (B) *endo*-5-isopropylnorbornene, (C) *exo*-5-ethylnorbornene, and (D) *exo*-5-isopropylnorbornene

respectively (Table 4). This results in a slower reaction as observed for the *exo*-5-isopropyl- and exo-5-t-butylnorbornenes in both the computational and experimental rates.

The observed lack of epimerization in the 7-alkylbicyclo[3.2.0]hept-2-enes might be attributed to (1) a significant difference in energy between the *endo* and *exo* stereoisomers that favors the *exo* epimer thermodynamically and/or (2) as Carpenter suggested, the presence of rotational bias from the angular momentum following the breaking of the C1-C7 bond.[10,14,15] A comparison of the computational enthalpy of formation values (Tables 4 and S3) shows that for most of the alkyl substituents, the *endo* epimer is actually lower in energy. The difference in enthalpy of formation ($\Delta\Delta H_f$) between the two stereoisomers is in most cases less than 2 kJ/mol, which is well within the 95% CI for the methods used here. These results are consistent with Tao and Fang,[17] who reported values for the *endo* and *exo*-5-methylnorbornenes that were within 0.4 to 1.7 kJ/mol of each other, with the *endo* being lower in energy.

The exceptions to this are the bulky isopropyl and *t*-butyl substituents, which give very different results. In the case of the isopropyl group, the *endo* epimers are 3.68 and 4.15 kJ/mol more stable than the *exo* epimers for the 7-isopropylbicyclo[3.2.0]hept-2-ene and 5-isopropylnorbornene, respectively. By adding an additional methyl group onto C8, converting isopropyl to *t*-butyl, the opposite trend is observed with the *exo* epimers being 5.72 and 1.87 kJ/mol more stable than the *endo* epimers of 7-*t*-butylbicyclo[3.2.0]hept-2-ene and 5-*t*-butylnorbornene, respectively. The reason for this can be seen in the steric interactions of the alkyl groups with the rigid ring structures. In the case of 7-isopropylbicyclo[3.2.0]hept-2-enes, the C1-C7-C6 bond angle is roughly 89° (Figure 2A,C). This acute angle allows the C1-C7-C8 bond angle to expand to roughly 120° and 116° for the *endo* and *exo* stereoisomers, respectively. The broad angle of the *endo* epimer moves much of the alkyl chain away from the ring structure, thereby reducing the steric interactions. At the same time, in the lowest energy conformers for both the *exo* and *endo* epimers, the alkyl chains have C1-C7-C8-C9 dihedral angles that are roughly 170° to 180°, which further reduces any steric effect of the alkyl group with the concave pocket of the bicyclic ring structure. For 7-isopropylbicyclo[3.2.0]hept-2-ene, it is the interaction between C1 and C10 that likely results in the destabilization of the *exo* epimer compared with the *endo* epimer. The C1..C10 distance in the *exo* epimer is 3.198 Å versus 3.632 Å for the *endo* epimer. The introduction of an additional methyl group on the alkyl group (C11 in Figure 2B,D), yielding 7-*t*-butylbicyclo[3.2.0]hept-2-ene, introduces significant steric effects, particularly for the *exo* epimer. The greater broadening of the C1-C7-C8 bond angle in *endo*-7-*t*-butylbicyclo[3.2.0]hept-2-ene going from 120.4° to 124.7° as compared with *exo*-7-*t*-bicyclo[3.2.0]hept-2-ene expanding from 116.2° to 118.2° is indicative of the effect of the stronger steric repulsion experienced by the new methyl groups. While the isopropyl was able to minimize the steric interaction with the ring by directing the methyl groups away from the ring and having the hydrogen pointed toward the ring, for *t*-butyl the new methyl group is located in the concave pocket of the bicyclo[3.2.0]hept-2-ene to which it is attached.

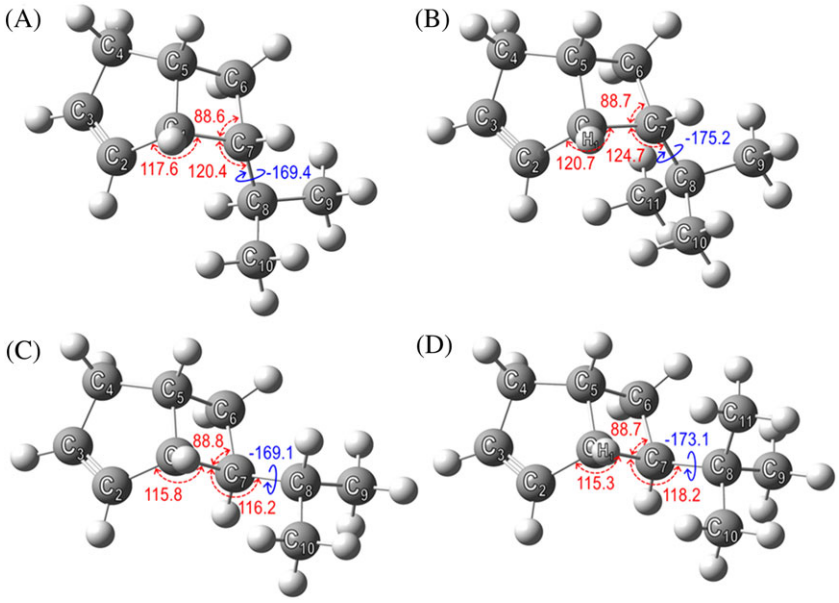

FIGURE 2 Molecular images with select geometric parameters for (A) *endo*-7-isopropylbicyclo[3.2.0]hept-2-ene, (B) *endo*-7-*t*-butylbicyclo[3.2.0]hept-2-ene, (C) *exo*-7-isopropylbicyclo[3.2.0]hept-2-ene, and (D) *exo*-7-*t*-butylbicyclo[3.2.0]hept-2-ene

A similar trend is observed for the 5-alkylnorbornenes. The *endo* epimers tend to be lower in energy, partially because the C4-C5-C8 bond angles are so broad (Figure 3) as well as the ability of the alkyl chain to move C9 and C10 away from the ring altogether. As with the 7-*t*-butylbicyclo[3.2.0]hept-2-enes, when the hydrogen on C8 is replaced with a methyl group, the resultant C11 in endo-5-*t*-butylnorbornene (Figure 3B,D) experiences greater steric interactions with the ring structure than in the *exo* epimer. The fact that the *endo* epimer is actually lower in energy for all of the alkyl chains except *t*-butyl means that the lack of epimerization in *exo*-7-alkylbicyclo[3.2.0]hept-2-enes is not the result of the *exo* epimer being significantly lower in energy. Instead, the observed thermodynamic favorability of the *endo* epimer gives greater credence to Carpenter's hypothesis that the rotational inertia of the alkyl group following cleavage of the C1-C7 bond in 7-alkylbicyclo[3.2.0]hept-2-enes is responsible for the observed stereoselectivity of the [1,3] sigmatropic rearrangement.[10,14,15]

While there is no obvious trend in the overall kinetic order, the % [1,3] product composition decreases and the % direct fragmentation increases incrementally as a function of alkyl mass for the series of unbranched substituents: -Me, -Et, -Pr, -Bu (Figure 4A,B).

The larger the alkyl mass, the greater the extent of fragmentation at the expense of [1,3] rearrangement. The absence of a global trend related to how the resultant non-equilibrated singlet diradicals bifurcate between rearrangement and fragmentation (Scheme 7) suggests multiple operative factors once the initial transition structure is reached and the intermediate begins to sample the

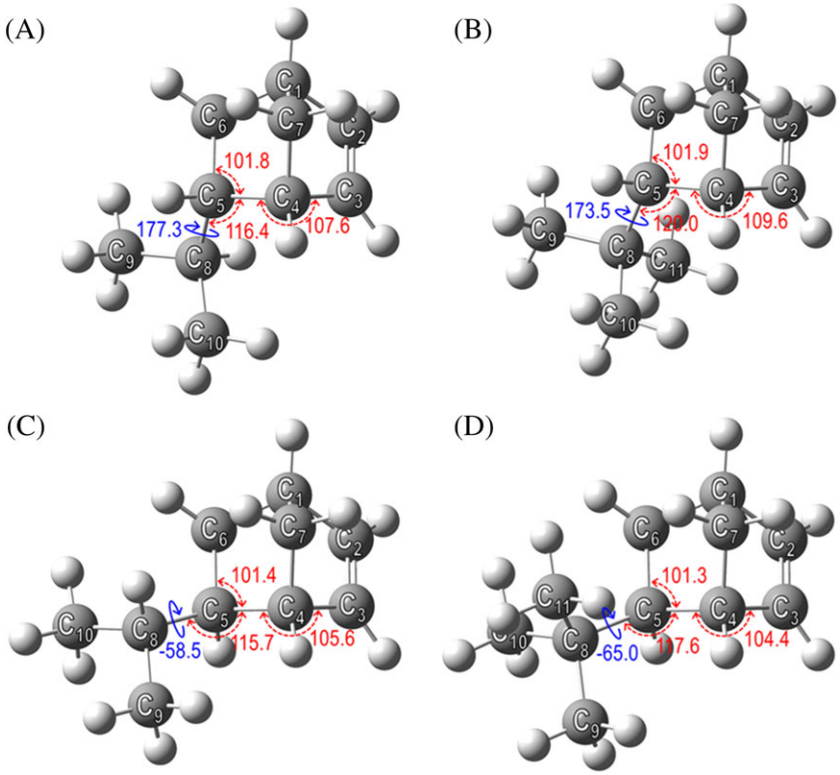

FIGURE 3 Molecular images with select geometric parameters for (A) *endo*-5-isopropylnorbornene, (B) *endo*-5-*t*-butylnorbornene, (C) *exo*-5-isopropylnorbornene, and (D) *exo*-5-*t*-butylnorbornene

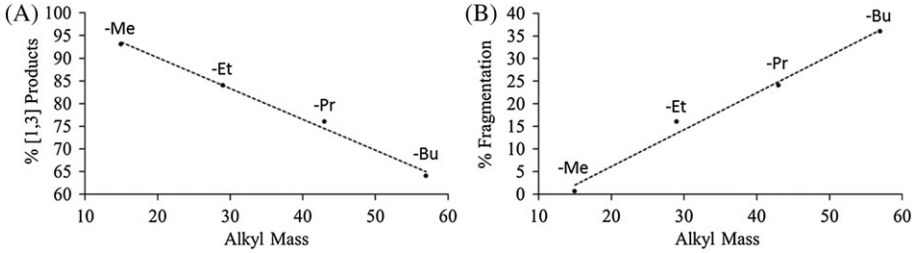

FIGURE 4 (A) % [1,3] products as a function of mass of alkyl group at C-7; (B) % fragmentation as a function of mass of alkyl group at C-7

TABLE 5 Stereoselectivity of [1,3] carbon shifts in *exo*-7-alkylbicyclo[3.2.0]hept-2-enes

R-	k_{si}	k_{sr}	si/sr	*%si*	*%sr*
Et-	1.2×10^{-5} s^{-1}	1.5×10^{-6} s^{-1}	8.0	89	11
i-Pr-	6.5×10^{-6} s^{-1}	8.1×10^{-7} s^{-1}	8.0	89	11
Me-	1.2×10^{-5} s^{-1}	1.9×10^{-6} s^{-1}	6.8	87	13
Pr-	1.3×10^{-5} s^{-1}	2.2×10^{-6} s^{-1}	5.9	86	14
Bu-	9.7×10^{-6} s^{-1}	1.8×10^{-6} s^{-1}	5.4	84	16
t-Bu-	8.3×10^{-6} s^{-1}	2.1×10^{-6} s^{-1}	4.0	80	20

available conformational space. For example, *exo*-7-isopropylbicyclo[3.2.0]hept-2-ene and *exo*-7-t-butylbicyclo[3.2.0]hept-2-ene with the bulkiest alkyl substituents react more slowly than other *exo*-7-alkylbicyclo[3.2.0]hept-2-enes. The former, however, reacts slower and fragments more than the latter. Carpenter stresses that the diradical intermediate undergoes substantial geometric changes once it arrives on the caldera, so it is not unreasonable to expect that numerous dynamic factors are at play.[14] Regardless of the size or mass of the alkyl group, the [1,3] rearrangement process dominates fragmentation by a factor of ca. 2:1 or greater, so that $k_{13} > k_f$ for all alkyl substituents. The k_{13}/k_f ratios are, however, much lower for all entries compared with that of *exo*-7-methylbicyclo[3.2.0]hept-2-ene (**3**) (Table 1). Thus, the methyl model for the bicyclo[3.2.0]hept-2-ene to norbornene thermal rearrangement is ironically an outlier.

The stereoselectivity of the [1,3] carbon shift as indicated by the *si*/*sr* ratio varies from 4 to 8, but the *%si* product contribution remains relatively constant. Examining the % contributions of the *si* and *sr* products directly (Table 5) reveals that the *si* product is highly favored, consistent with the predictions of Carpenter[10] and Houk[11]. The *%si* range varies narrowly from 80% to 89%, an outcome dictated by preservation of the moment of inertia once the endo trajectory commences.[11]

4 | CONCLUSIONS

High-level composite methods were used to determine the enthalpy differences between a series of *endo*- and *exo*-7-alkylbicyclo[3.2.0]hept-2-enes, *endo*- and *exo*-5-alkylnorbornenes and the rate parameters for retro Diels-Alder reactions thereof. The computational and experimental rate values are in good agreement, particularly for the relative reactivity of the *endo* versus *exo* epimers. The *exo* epimers were found to be less reactive due to higher energy transition states caused by steric interactions of the alkyl groups with C4 and C7 in the transition state. This effect is stronger for the branched isopropyl and *t*-butyl groups. Surprisingly, the *endo* epimers of both the 7-alkylbicyclo[3.2.0]hept-2-enes and 5-alkylnorbornenes were determined to be lower in energy, except for the *t*-butyl group, for which the exo epimer is lower in energy. This trend is attributed to the narrow C-C-C bond angles in the ring structures, which results in a widening of the C-C-C bond angle of the alkyl group. This aligns the alkyl groups away from the concave pocket in the *endo* epimers and leads to a lowering of steric interactions. Because the *endo* epimer is lower in energy, the lack of epimerization that is observed experimentally is attributed to a rotational inertia bias, described originally by Carpenter,[10] that leads to preferential formation of the exo-5-alkylnorbornenes.

According to Houk,[31] "initial trajectories of bond rotations" exert the most pronounced effect on product distributions. Once the C1-C7 bond breaks, as shown in Scheme 7, an endo trajectory of the migrating carbon C7 would propel it toward the migration terminus C3, whereas an exo trajectory of the migrating carbon C7 would favor fragmentation. The data in Table 1 and Figure 4 suggest that *exo*-7-alkylbicyclo[3.2.0]hept-2-enes, as the size of the alkyl group increases, undergo more exo trajectories to yield a greater proportion of fragmentation. Thus, the %fragmentation increases from 0.6% for *exo*-7-methylbicyclo[3.2.0]hept-2-ene to 36% for *exo*-7-butylbicyclo[3.2.0]hept-2-ene, which might well be attributable to a steric effect between the hydrogen on C1 and other hydrogens on the alkyl chain that could disfavor the endo trajectory.

Based on numerous computational studies,[10,17,31] the assumption of a shallow energy minimum for the diradical intermediate in Scheme 7 on a potential energy surface described as a "caldera" is highly plausible. A recent reappraisal of Carpenter's "dynamical matching" phenomenon for bicyclo[3.2.0]hept-2-ene and its C7-methyl analog has led to "generalized dynamic matching" for singlet diradicals on a caldera generated from both classical and quantum dynamic models of the potential energy surface.[15] Fundamentally, the strong preference for the *si* over the sr product (Table 5) confirms that the singlet diradical intermediate experiences momentum direction, which is merely a "manifestation of the First Law of Motion," once the endo trajectory[31] commences.

Although Nohira and Nohira[32] have extended conservation of orbital symmetry theory to [1,3] sigmatropic rearrangements by generating a correlation diagram for the **1**-to-**2** transformation reported by Berson and Nelson,[5] as depicted earlier (Equation 1), by violating the noncrossing rule, this paradigm does not dictate adherence to conservation of orbital symmetry. We have

provided experimental and computational evidence to support the conclusion that [1,3] carbon migrations, such as those reported herein, are governed by conservation of angular momentum, wherein the moment of inertia resists deflection once the [1,3] carbon migration is initiated. Thus, conservation of orbital symmetry does not account for the apparent stereoselectivity of [1,3] sigmatropic rearrangements of *exo*-7-alkylbicyclo[3.2.0]hept-2-enes.

ACKNOWLEDGEMENTS

Acknowledgment is made to the donors of the American Chemical Society Petroleum Research Fund and the Franklin & Marshall College Hackman Fund for support of this research, and to King Abdullah University of Science and Technology supercomputing laboratory for access to their computing resources.

ORCID

Phyllis Leber http://orcid.org/0000-0002-6044-5664
Alexander Davis http://orcid.org/0000-0001-8966-234X

REFERENCES

[1] H. M. Frey, A. T. Cocks, *J. Chem. Soc. A* **1971**, 2564.

[2] J. D. Bender, P. A. Leber, R. R. Lirio, R. S. Smith, *J. Org. Chem.* **2000**, *65*, 5396.

[3] R. B. Woodward, R. Hoffmann, *The Conservation of Orbital Symmetry*, Verlag Chemie, Weinheim **1970** 119.

[4] J. J. Gajewski, *Acc. Chem. Res.* **1980**, *13*, 142.

[5] J. A. Berson, G. L. Nelson, *J. Am. Chem. Soc.* **1967**, *89*, 5503.

[6] J. E. Baldwin, P. A. Leber, *Org. Biomol. Chem.* **2008**, *6*, 36.

[7] J. A. Berson, *Acc. Chem. Res.* **1972**, *5*, 406.

[8] G.-G. Klärner, R. Drewes, D. Hasselmann, *J. Am. Chem. Soc.* **1988**, *110*, 297.

[9] J. E. Baldwin, K. D. Belfield, *J. Am. Chem. Soc.* **1988**, *110*, 296.

[10] B. K. Carpenter, *J. Am. Chem. Soc.* **1995**, *117*, 6336.

[11] S. Wilsey, K. N. Houk, A. H. Zewail, *J. Am. Chem. Soc.* **1999**, *121*, 5772.

[12] B. R. Beno, S. Wilsey, K. N. Houk, *J. Am. Chem. Soc.* **1999**, *121*, 4816.

[13] P. B. Karadakov, D. L. Cooper, A. Uhe, *Int. J. Quant. Chem.* **2009**, *109*, 1807.

[14] B. K. Carpenter, *Chem. Rev.* **2013**, *113*, 7265.

[15] P. Collins, Z. C. Kramer, B. K. Carpenter, G. S. Ezra, S. Wiggins, *J. Chem. Phys.* **2014**, *141*, 034111/1.

[16] P. A. Leber, C. C. Lasota, N. A. Strotman, G. S. Yen, *J. Org. Chem.* **2007**, *72*, 912.

[17] H.-R. Tao, D.-C. Fang, *Theor. Chem. Acc.* **2008**, *121*, 91.

[18] M. Rey, S. Roberts, A. Dieffenbacher, A. S. Dreiding, *Helv. Chim. Acta* **1970**, *53*, 417.

[19] J. D. Burkey, P. A. Leber, L. S. Silverman, *Synth. Commun.* **1986**, *16*, 1363.

[20] N. Windmon, V. Dragojlovic, *Green Chem. Lett. Rev.* **2008**, *1*, 155.

[21] H. Koch, W. Haaf, *Liebigs Ann. Chem.* **1960**, *638*, 111.

[22] M. J. Frisch, G. W. Trucks, H. B. Schlegel, G. E. Scuseria, M. A. Robb, J. R. Cheeseman, G. Scalman, V. Barone, B. Mennucci, G. A. Petersson, H. Nakatsuji, M. Caricato, X. Li, H. P. Hratchian, A. F. Izmaylov, J. Bloino, G. Zheng, J. L. Sonnenberg, M. Hada, M. Ehara, K. Toyota, R. Fukuda, J. Hasegawa, M. Ishida, T. Nakajima, Y. Honda, O. Kitao, H. Nakai, T. Vreven, J. A. Montgomery Jr., J. E. Peralta, F. Ogliaro, M. J. Bearpark, J. Heyd, E. N. Brothers, K. N. Kudin, V. N. Staroverov, R. Kobayashi, J. Normand, K. Raghavachari, A. P. Rendell, J. C. Burant, S. S. Iyengar, J. Tomasi, M. Cossi, N. Rega, N. J. Millam, M. Klene, J. E. Knox, J. B. Cross, V. Bakken, C. Adamo, J. Jaramillo, R. Gomperts, R. E. Stratmann, O. Yazyev, A. J. Austin, R. Cammi, C. Pomelli, J. W. Ochterski, R. L. Martin, K. Morokuma, V. G. Zakrzewski, G. A. Voth, P. Salvador, J. J. Dannenberg, S. Dapprich, A. D. Daniels, Ö. Farkas, J. B. Foresman, J. V. Ortiz, J. Cioslowski, D. J. Fox in Gaussian, Inc.: Wallingford, CT, USA, **2009**.

[23] A. D. Becke, *J. Chem. Phys.* **1993**, *98*, 5648.

[24] C. Lee, W. Yang, R. G. Parr, *Phys. Rev. B.* **1998**, *37*, 785.

[25] J. A. Montgomery Jr., M. J. Frisch, J. W. Ochterski, G. A. Petersson, *J. Chem. Phys.* **2000**, *112*, 6532.

[26] L. A. Curtiss, K. Raghavachari, P. C. Redfern, V. Rassolov, J. A. Pople, *J. Chem. Phys.* **1998**, *109*, 7764.

[27] L. A. Curtiss, P. C. Redfern, K. Raghavachari, *J. Chem. Phys.* **2007**, *127*, 124105.

[28] K. P. Somers, J. M. Simmie, *J. Phys. Chem. A* **2015**, *119*, 8922.

[29] V. Mokrushin, V. Bedanov, W. Tsang, M. Zachariah, V. Knyazev, W. McGivern National Institute of Standards and Testing, Gaithersburg, MD, **2009**.

[30] K. S. Pitzer, W. D. Gwinn, *J. Chem. Phys.* **1942**, *10*, 428.

[31] B. H. Northrop, K. N. Houk, *J. Org. Chem.* **2006**, *71*, 3.

[32] H. Nohira, T. Nohira, *J. Theor. Comput. Chem.* **2017**, *26*. 1750055-1750051

SUPPORTING INFORMATION

Additional supporting information may be found online in the Supporting Information section at the end of the article.

How to cite this article: Leber P, Kidder K, Viray D, Dietrich-Peterson E, Fang Y, Davis A. Stereoselectivity in a series of 7-alkylbicyclo[3.2.0] hept-2-enes: Experimental and computational perspectives. *J Phys Org Chem*. 2018;e3888. https://doi.org/10.1002/poc.3888